J|A|C|S
ARTICLES
Published on Web 03/30/2006

DABCO-Induced Self-Assembly of a Trisporphyrin Double-Decker Cage: Thermodynamic Characterization and Guest Recognition

Pablo Ballester,*,† Ana I. Oliva,§ Antoni Costa,‡ Pere M. Deyà,‡ Antonio Frontera,‡ Rosa M. Gomila,‡ and Christopher A. Hunter*,¶

Contribution from the Institució Catalana de Recerca i Estudis Avançats (ICREA) and Institute of Chemical Research of Catalonia (ICIQ), 43007-Tarragona, Spain, Departament de Química, Universitat de les Illes Balears, 07122-Palma de Mallorca, Spain, and Centre for Chemical Biology, Krebs Institute for Biomolecular Science, Department of Chemistry, University of Sheffield, Sheffield S3 7HF, U.K.

Received January 26, 2006; E-mail: pballester@iciq.es

Abstract: This paper describes the thermodynamic characterization of the self-assembly of a Zn trisporphyrin induced by coordination with 1,4-diazabicyclo[2.2.2]octane (DABCO) to form a stable 2:3 double-decker molecular coordination cage that recognizes benzene-1,3,5-tricarboxamides. The self-assembly process has been studied using UV−vis and ^{1}H NMR spectroscopy and quantitatively characterized in terms of a single stability constant that describes the strength of the individual coordination interactions and two effective molarities (EM) that describe the additional stability imparted by intramolecular cyclization. The EM values of the two consecutive cyclic intramolecular interactions are very similar. At micromolar concentrations, the formation of the fully assembled coordination cage is highly favored over the formation of intermediate species stabilized by fewer interactions, and so self-assembly is an all-or-nothing process. In contrast, at millimolar concentrations, the relative stability of intermediate species increases, leading to a stepwise self-assembly process, and a 2:2 intermediate can be clearly identified using ^{1}H NMR spectroscopy. The molecular recognition of benzene-1,3,5-tricarboxamides by the cage was investigated using ^{1}H NMR spectroscopy. The tricarboxamides bind inside the central cavity of the cage complex, and isothermal titration calorimetry (ITC) allowed the quantification of the stoichiometry and binding affinities.

Introduction

Self-assembly has been described in one of its many definitions as "the process by which specific components spontaneously assemble in a highly selective fashion into a well-defined, discrete supramolecular architecture".[1] For self-assembly processes in which the product is stable under thermodynamic equilibration, Lindsey has coined the term "strict self-assembly".[2] Several authors have suggested that a prerequisite for the construction of a well-defined and discrete supramolecular architecture resulting from strict self-assembly is the establishment of multiple and separated connections operating in one or more closed loops[3−5] (multivalency or multitopicity). The interaction that closes a loop becomes intramolecular even when it is taking place between complementary binding sites pertaining to different molecules, if a previous noncovalent intermolecular interaction between them is present. The binding constant of a strainless intramolecular interaction can be related to the product of the intrinsic binding constant for the individual interaction and an effective concentration (or effective molarity, EM) term which accounts for the close proximity of the interacting (reacting) groups.[6−9] The EM is an empirical parameter derived from the ratio of stability or rate constants for intra- and intermolecular events. Assuming a strainless intramolecular reaction, the value of EM turns out to be mostly dependent on the number of single rotatable bonds in the chain.[10,11] These data indicate that the self-assembly of strainless

† ICREA and ICIQ.
§ ICIQ.
‡ Universitat de les Illes Balears.
¶ University of Sheffield.

(1) Pfeil, A.; Lehn, J. M. *J. Chem. Soc., Chem. Commun.* **1992**, 838−40.
(2) Lindsey, J. S. *New J. Chem.* **1991**, *15*, 153−80.
(3) Taylor, P. N.; Anderson, H. L. *J. Am. Chem. Soc.* **1999**, *121*, 11538−11545.
(4) (a) Ercolani, G. *J. Phys. Chem. B* **2003**, *107*, 5052−5057. (b) Ercolani, G. *J. Phys. Chem. B* **1998**, *102*, 5699−5703.
(5) (a) Chi, X. L.; Guerin, A. J.; Haycock, R. A.; Hunter, C. A.; Sarson, L. D. *J. Chem. Soc., Chem. Commun.* **1995**, 2563−2565. (b) Chi, X. L.; Guerin, A. J.; Haycock, R. A.; Hunter, C. A.; Sarson, L. D. *J. Chem. Soc., Chem. Commun.* **1995**, 2567−2569.
(6) Mulder, A.; Auletta, T.; Sartori, A.; Del Ciotto, S.; Casnati, A.; Ungaro, R.; Huskens, J.; Reinhoudt, D. N. *J. Am. Chem. Soc.* **2004**, *126*, 6627−6636.
(7) Mulder, A.; Huskens, J.; Reinhoudt, D. N. *Org. Biomol. Chem.* **2004**, *2*, 3409−3424.
(8) Gargano, J. M.; Ngo, T.; Kim, J. Y.; Acheson, D. W. K.; Lees, W. J. *J. Am. Chem. Soc.* **2001**, *123*, 12909−12910.
(9) Menozzi, E.; Rebek, J. *Chem. Commun.* **2005**, 5530−5532.
(10) Cacciapaglia, R.; Di Stefano, S.; Mandolini, L. *Acc. Chem. Res.* **2004**, *37*, 113−122.
(11) Jacobson, H.; Stockmayer, W. H. *J. Chem. Phys.* **1950**, *18*, 1600−1606. See also ref 8.

10.1021/ja060608t CCC: $33.50

medium-size macrocycles can occur with a relatively high value of EM, which is slightly affected by the size of the cycle. The EM values quantify the cyclization tendency since they represent the (sometimes hypothetical) concentration of the interaction centers needed for the intermolecular process (polymerization) to compete effectively with the intramolecular counterpart (self-assembly of the macrocycle). The high values of EM for medium-size macrocyclization processes, together with the possibility of increasing the driving force of self-assembly by increasing the strength of the intermolecular interaction and the degree of cyclicity of the supramolecular architecture, make this phenomenon an attractive alternative to the covalent and kinetically controlled synthesis of macrocyclic receptors. Furthermore, the covalent synthesis of macrocyclic receptors is usually a very tedious and low yielding process, requiring high dilution conditions and extensive chromatographic purifications. This is due to the fact that, during the covalent synthesis of macrocycles, the products are often kinetically trapped in undesired structures. The thermodynamic control operative in the strict self-assembly of macrocycles eliminates this problem, implying that under certain conditions a discrete and unique species, the most "stable",[12] can be quantitatively formed in solution. In fact, a great variety of macro- and oligocyclic supramolecular architectures have been obtained using multimolecular self-assembly processes.[13−15] Many such materials are interesting as artificial molecular receptors and supramolecular catalysts.[16−18] However, detailed thermodynamic characterization of the self-assembly process and quantitative assessment of the robustness of the architecture assembled in solution remain limited. Herein we report a detailed account of the self-assembly of a Zn trisporphyrin induced by coordination with 1,4-diazabicyclo[2.2.2]octane (DABCO) to form a stable double-decker molecular cage **7**, featuring an internal cavity big enough to be used as a molecular receptor.[19]

Results and Discussion

Reference Models. As reference model systems to assist in the study of the self-assembly of the zinc trisporphyrin **1**, we use the binding interactions of a zinc metalated monoporphyrin (5,10,15,20-tetrakis(4-pentylphenyl)porphyrin, **2**) and a zinc bisporphyrin (5-methoxy-*N*,*N*′-bis[4-[10,15,20-tris(4-pentylphenyl)porphin-5-yl]phenyl]-1,3-benzenecarboxamide, **3**) with 1,4-diazabicyclo[2.2.2]octane **4** (DABCO) (see Figure 1). We have previously described in detail the binding properties of **2** and **3** with **4** in chloroform solution using ^{1}H NMR and UV−vis spectroscopy.[20] Below we will summarize the findings that are relevant to the present study.

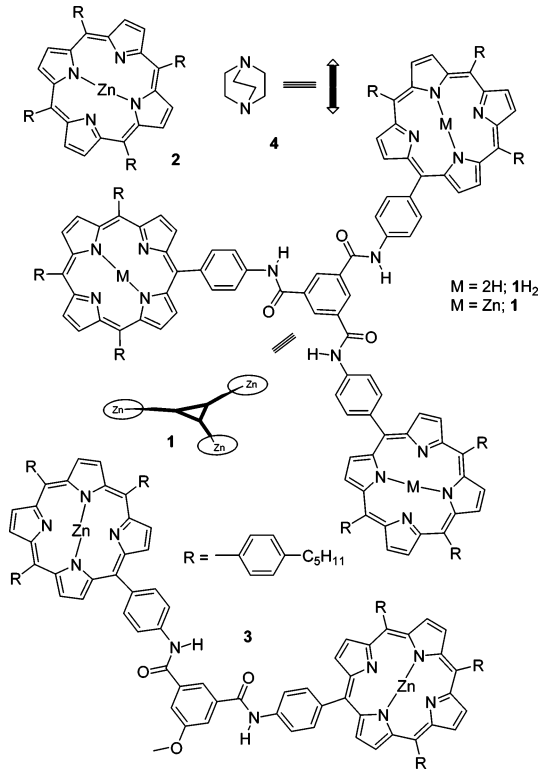

Figure 1. Structures of the porphyrin systems used in this study and of the ligand DABCO.

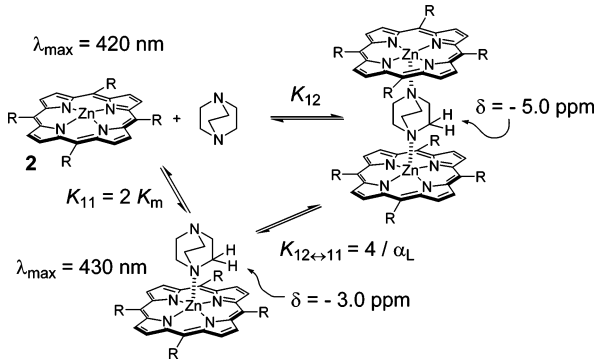

Figure 2. Species and equilibria involved in the complexation of DABCO with monoporphyrin **2**. Some characteristic spectroscopic data are indicated for each species. K_{12} is the overall stability constant for the formation of DABCO·**2**$_2$ (1:2) complex. K_{11} refers to the stability constant of DABCO·**2** (1:1) complex. $K_{12\leftrightarrow 11}$ is the equilibrium constant for the destruction of the DABCO·**2**$_2$ (1:2) sandwich complex in the presence of excess DABCO to yield DABCO·**2** (1:1) complex.

A. Binding of DABCO to Monoporphyrin 2: The equilibrium constants shown in Figure 2 and mentioned above in the text of this section are defined as follows:

$$K_{11} = [\text{DABCO}\cdot\mathbf{2}]/[\text{DABCO}][\mathbf{2}]$$

$$K_{12} = [\text{DABCO}\cdot\mathbf{2}_2]/[\text{DABCO}][\mathbf{2}]^2$$

$$K_{12\leftrightarrow 11} = (K_{11})^2/K_{12} = [\text{DABCO}\cdot\mathbf{2}]^2/[\text{DABCO}\cdot\mathbf{2}_2][\text{DABCO}]$$

When the coordination of DABCO with **2** is studied with UV−vis spectroscopy (porphyrin concentration ∼ 10^{-6} M), the

(12) Mammen, M.; Simanek, E. E.; Whitesides, G. M. *J. Am. Chem. Soc.* **1996**, *118*, 12614−12623. The "stability" of a multimolecular assembly is not reflected simply in the magnitude of $\Delta G°$ since the effect of concentration on favoring its formation is not indicated in $\Delta G°$.
(13) Fujita, M.; Tominaga, M.; Hori, A.; Therrien, B. *Acc. Chem. Res.* **2005**, *38*, 369−378.
(14) Seidel, S. R.; Stang, P. J. *Acc. Chem. Res.* **2002**, *35*, 972−983.
(15) Caulder, D. L.; Raymond, K. N. *Acc. Chem. Res.* **1999**, *32*, 975−982.
(16) (a) Crowley, J. D.; Goshe, A. J.; Bosnich, B. *Chem. Commun.* **2003**, 2824−2825. (b) Mateos-Timoneda, M. A.; Kerckhoffs, J.; Crego-Calama, M.; Reinhoudt, D. N. *Angew. Chem., Int. Ed.* **2005**, *44*, 3248−3253.
(17) Fiedler, D.; Bergman, R. G.; Raymond, K. N. *Angew. Chem., Int. Ed.* **2004**, *43*, 6748−6751.
(18) Fiedler, D.; Leung, D. H.; Bergman, R. G.; Raymond, K. N. *Acc. Chem. Res.* **2005**, *38*, 349−358.
(19) For other examples of DABCO-induced self-assembly, see: (a) Hunter, C. A.; Tregonning, R. *Tetrahedron* **2002**, *58*, 691−697. (b) Baldini, L.; Ballester, P.; Casnati, A.; Gomila, R. M.; Hunter, C. A.; Sansone, F.; Ungaro, R. *J. Am. Chem. Soc.* **2003**, *125*, 14181−14189. (c) See also, refs 3, 20, and 24.
(20) Ballester, P.; Costa, A.; Castilla, A. M.; Deyà, P. M.; Frontera, A.; Gomila, R. M.; Hunter, C. A. *Chem.−Eur. J.* **2005**, *11*, 2196−2206.

exclusive formation of axial coordinated complexes with a 1:1 stoichiometry ($K_{11} = 1.3 \pm 0.1 \times 10^5$ M^{-1}) is observed. The binding of DABCO induces a shift of the Soret band of **2** from 420 to 430 nm. When the same system is studied using ^{1}H NMR spectroscopy (porphyrin concentration $\sim 10^{-3}$ M), 1:1 and 1:2 complexes can be detected. The chemical shift of the methylene protons of the complexed DABCO is diagnostic of the stoichiometry. Thus, the ternary complex DABCO·**2**$_2$ can be characterized by a signal at approximately $\delta = -5$ ppm corresponding to the six methylene protons of the DABCO sandwiched between two porphyrin units. A DABCO signal at $\delta = -3$ ppm is indicative of the binary complex DABCO·**2** and can be assigned to the three methylene groups in the α-position with respect to the nitrogen bound to the zinc porphyrin (Figure 2). In the presence of more than 0.5 equiv of DABCO, the DABCO signals due to the 1:1 and 1:2 complexes are in slow exchange on the NMR time scale at low temperature (220 K). However, at room temperature, only the signal at $\delta = -5$ ppm is observed. When more DABCO is added, the signal at $\delta = -5$ ppm broadens and finally disappears due to chemical exchange. The equilibrium constant ($K_{12\leftrightarrow11}$) for the destruction of the ternary complex by excess DABCO was determined by ^{1}H NMR titration and used to quantify the cooperativity between the two binding sites of DABCO on forming the DABCO·**2**$_2$ complex. A value of $\alpha_L = 0.8 \pm 0.2$ was determined, indicating that there is rather little cooperativity in the formation of the sandwich complex.

B. Binding of DABCO to Bisporphyrin 3: The overall stability constant of individual species in which **3** is involved and the equilibrium constant $K_{22\leftrightarrow21}$ shown in Figure 3 are defined as follows:

$$K_{21} = [(\text{DABCO})_2\cdot\mathbf{3}]/[\text{DABCO}]^2[\mathbf{3}]$$

$$K_{22} = [(\text{DABCO})_2\cdot\mathbf{3}_2]/[\text{DABCO}]^2[\mathbf{3}]^2$$

$$K_{22\leftrightarrow21} = (K_{21})^2/K_{22} = [(\text{DABCO})_2\cdot\mathbf{3}]^2/[[(\text{DABCO})_2\cdot\mathbf{3}_2][\text{DABCO}]^2]$$

The initial addition of DABCO to a chloroform solution of **3** (porphyrin concentration $\sim 10^{-6}$ M) leads to a shift of the Soret absorption from 420 to 426 nm in the UV−vis spectrum. This 6 nm red shift of the Soret band is characteristic of the formation of DABCO sandwich complexes.[21] On addition of more DABCO, the intensity of the band at 426 nm decreases and a new band appears at 431 nm. The Soret absorption at 431 nm is typical of a 1:1 DABCO−porphyrin complex. This result suggests that two consecutive two-state equilibria are present and that it is valid to analyze the UV titration data in terms of three colored species involving **3**. It is worth mentioning that the titration shows a sharp isosbestic point at the beginning followed by a nonisosbestic middle phase and the appearance of a new isosbestic point at the end. When complexation is studied using ^{1}H NMR spectroscopy at room temperature, in the presence of less than 1 equiv of DABCO, the methylene protons due to bound DABCO appear at approximately $\delta = -5$ ppm, which is diagnostic of the formation of a sandwich complex. As more DABCO is added, the signal at −5 ppm broadens due to chemical exchange. During this fast exchange phase of the titration, it is possible to quantify the amount of sandwich complex present using the changes in chemical shift experienced by the protons of bisporphyrin **3**. The NMR data agree well with simulated speciation profiles derived from the stability constants determined in the UV−vis titration and demonstrate that bisporphyrin **3** forms exclusively a 2:2 (DABCO)$_2$·**3**$_2$ intermolecular sandwich complex which opens up to form a simple 2:1 (DABCO)$_2$·**3** complex in the presence of excess DABCO. The stability constant[22] of the 2:2 complex is $K_{22} = 6 \pm 2 \times 10^{18}$ M^{-3} corresponding to an EM = 0.3 ± 0.2 M[23] for the intramolecular event.

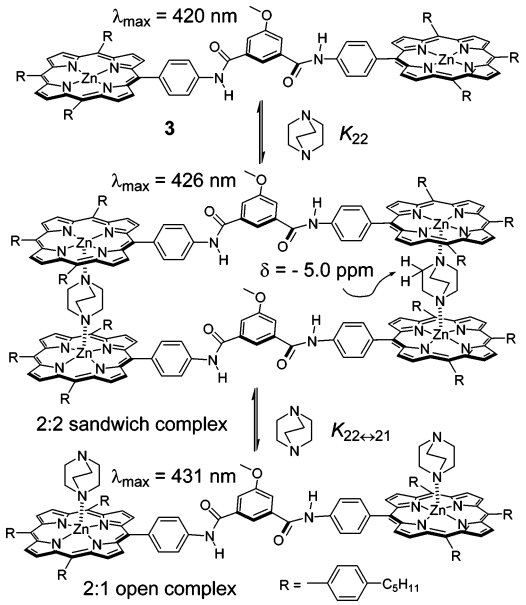

Figure 3. Species and equilibria involved in the complexation of DABCO with bisporphyrin **3**. Some characteristic spectroscopic data are indicated for each species. K_{22} is the overall stability constant for the formation of (DABCO)$_2$·**3**$_2$ (2:2) complex. $K_{22\leftrightarrow21}$ is the equilibrium constant for the destruction of the (DABCO)$_2$·**3**$_2$ (2:2) sandwich complex in the presence of excess DABCO to yield (DABCO)$_2$·**3** (2:1) complex.

Synthesis. The syntheses of monoporphyrin **2** and bisporphyrin **3** have been previously reported.[20] Trisporphyrin **1**H$_2$ was synthesized by dropwise addition of a methylene chloride solution of the triacid chloride **5** into another dichloromethane solution at 0 °C, containing 4 equiv of *para*-aminoporphyrin **6** and excess triethylamine. Column chromatography of the crude product allowed the isolation of trisporphyrin **1**H$_2$ in 67% yield. Metalation was accomplished by using a solution of zinc acetate in methylene chloride/methanol (3:1) followed by column chromatography on neutral alumina, yielding zinc trisporphyrin **1** in 87%. This product was recrystallized from methylene chloride/methanol and carefully dried in vacuo prior to being used in the binding experiments.

(21) Mak, C. C.; Bampos, N.; Sanders, J. K. M. *Angew. Chem., Int. Ed.* **1998**, *37*, 3020−3023.

(22) The small discrepancies between the stability constant values described in ref 20 and the ones reported here are probably due to differences in ethanol content of the chloroform used. The same batch of chloroform was used to carry out all the UV−vis titrations reported in this study. The measured value for $K_{21} = 9 \pm 1 \times 10^9$ M^{-2} can also be used to estimate a K_m value using the approximation $K_{21} = 4K_m^2$. The similarity between the obtained value 5×10^4 M^{-1} and that of the calculated microscopic binding constant for DABCO binding to **2** ($K_m = 6.5 \pm 0.5 \times 10^4$ M^{-1}) is a clear indication of the quality of the fit.

(23) This value was obtained using the formula EM = $K_{22}/\alpha_P\alpha_L K_m^4$. The cooperativity factors for the ligand and for the bisporphyrin were calculated to be equal to 1. See ref 20.

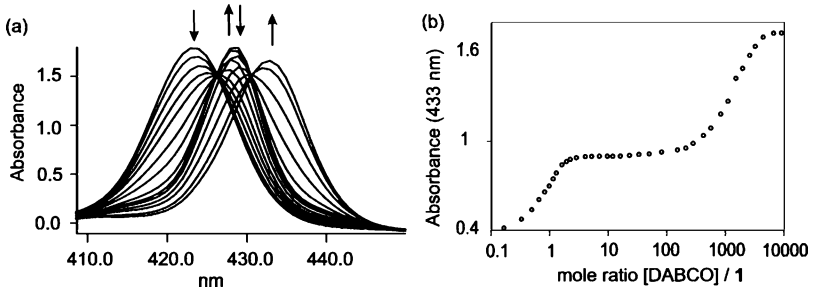

Figure 4. Titration of trisporphyrin **1** with DABCO in chloroform ([**1**] = 1×10^{-6} M): (a) selected absorption spectra during the course of the titration (number of DABCO equivalents added: 0, 0.16, 0.32, 0.48, 0.64, 0.96, 1.28, 1.90, 9.46, 277, 824, 1467, 3145, 8845); and (b) complexation isotherm at 433 nm, showing the three phases of the titration (rise of assembly **7**, concentration range of DABCO where **7** is stable, and finally dissociation of **7**) to yield the open complex **8** with excess of DABCO (see text for a more detailed explanation).

DABCO-Induced Self-Assembly of Trisporphyrin 1 into Cage Structure 7. The assembly of trisporphyrin **1** induced by DABCO coordination was first probed using UV−vis spectroscopy (porphyrin concentration $\sim 10^{-6}$ M).[24] The covalent connectivity of trisporphyrin **1**, analogous to that of bisporphyrin **2**, precludes the formation of intramolecular complexes with DABCO. Addition of DABCO to a chloroform solution of trisporphyrin **1** results in a series of isosbestic spectra with a concomitant shift of the Soret band originally centered at 423−429 nm. As mentioned above, this 6 nm red shift is characteristic of the formation of a DABCO sandwich complex. The maximum of the band at 429 nm reaches saturation after 7 equiv of DABCO is added. No further change of the absorbance is observed until 50 equiv of DABCO is added. From this point on, the spectra show a new sharp isosbestic point. The band at 429 nm decreased, and a new band appeared at 431 nm, typical of a Zn porphyrin monocoordinated to DABCO (Figure 4). It is worth mentioning that the nonisosbestic middle phase that we observed in the titration of **2**, which was indicative of the simultaneous formation and destruction of the assembly, is not observed with **1**. Taken together, these results indicate that even under the dilute conditions of the UV−vis titration (a) the assembly is fully formed, (b) the assembly is stable in the presence of a moderate excess of DABCO, and (c) the assembly starts to dissociate in a DABCO concentration regime that is quite different from that required for its formation.

We were able to analyze the titration data using global multivariate factor analysis[25] considering only three colored species (free trisporphyrin **1**, 3:2 assembly **7**, and 3:1 open complex **8**; see Scheme 2). The equilibrium constants considered in Scheme 2 are defined as follows:

$$K_{31} = [(\mathrm{DABCO})_3\cdot\mathbf{1}]/[\mathrm{DABCO}]^3[\mathbf{1}]$$

$$K_{32} = [(\mathrm{DABCO})_3\cdot\mathbf{1}_2]/[\mathrm{DABCO}]^3[\mathbf{1}]^2$$

$$K_{32\leftrightarrow 31} = (K_{31})^2/K_{32} = [(\mathrm{DABCO})_3\cdot\mathbf{1}]^2/[[(\mathrm{DABCO})_3\cdot\mathbf{1}_2][\mathrm{DABCO}]^3]$$

The fact that two phases of the titration show a clean isosbesticity is an indication that, under the dilute conditions used in the UV−vis titration, the concentrations of any intermediate colored species which may be involved during the formation or the destruction of the assembly are negligible. To minimize the number of variables in the fitting procedure, we decided to fix the UV−vis spectra of free **1** and of the open complex **8**, $(\mathrm{DABCO})_3\cdot\mathbf{1}$, using the initial and final spectra of the titration, respectively. In addition, the stability constant of the 3:1 complex was estimated using the value for the reference complex DABCO·**2** (K_m in Figure 2), so that $K_{31} = 8 \times K_m^3 = 2.2 \times 10^{15}$ M^{-3}.[26] The variables remaining to be optimized during the fitting of the data are the stability constant of the assembly **7**, K_{32}, and its UV−vis spectrum, which is well-defined by the plateau region in the middle of the titration. The

Scheme 1. Synthesis of Zn trisporphyrin **1**[a]

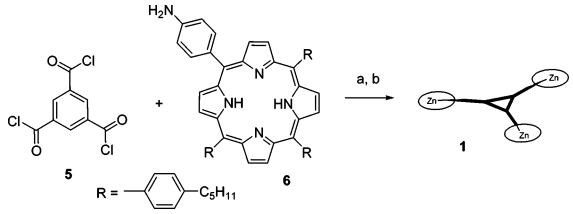

[a] Conditions: (a) CH_2Cl_2, 0 °C to room temperature; (b) $Zn(OAc)_2$ in $MeOH/CH_2Cl_2$ (1:3).

Scheme 2. Schematic Representation of the Species Involved in the Binding of DABCO to Trisporphyrin **1**[a]

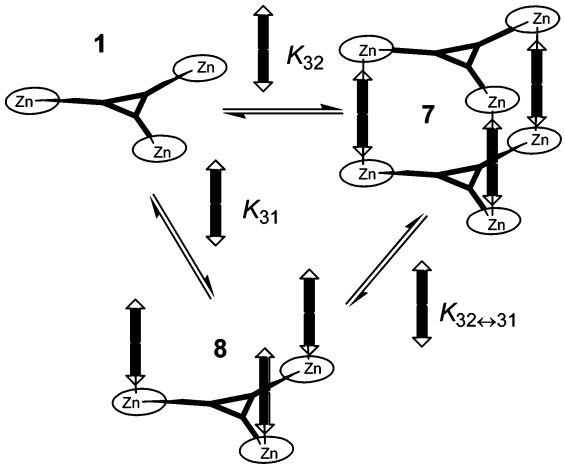

[a] K_{32} is the overall stability constant for the formation of **7**, $(\mathrm{DABCO})_3\cdot\mathbf{1}_2$ (3:2) cage complex. K_{31} is the overall stability constant for the formation of **8**, $(\mathrm{DABCO})_3\cdot\mathbf{1}$ (3:1) open complex. $K_{32\leftrightarrow 31}$ is the equilibrium constant for the destruction of cage **7** with excess DABCO to yield open complex **8**.

(24) A related multicomponent porphyrin assembly acting as functional bidentate ligand was described during the course of this work: Slagt, V. F.; van Leeuwen, P.; Reek, J. N. H. *Angew. Chem., Int. Ed.* **2003**, *42*, 5619−5623.

(25) (a) *SPECFIT*, version 3.0; Spectra Software Associates. (b) Gampp, H.; Maeder, M.; Meyer, C. J.; Zuberbühler, A. D. *Talanta* **1985**, *32*, 95−101. (c) Gampp, H.; Maeder, M.; Meyer, C. J.; Zuberbühler, A. D. *Talanta* **1986**, *33*, 943−951.

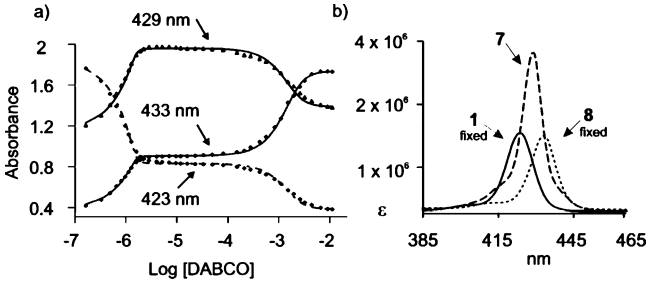

Figure 5. (a) UV−vis titration data (change in absorbance at three wavelengths, 423, 429, and 433 nm) for the binding of **1** with DABCO fitted to the calculated curves for the equilibria in Scheme 2. (b) UV−vis spectra for the three colored species in equilibrium.

calculated value for K_{32} is therefore based on the simultaneous fitting of the titration data for the formation of the assembly and for its destruction.

Figure 5 shows the excellent fit of the titration data to the binding model described in Scheme 2. The stability constant calculated for the cage is $K_{32} = (8 \pm 2) \times 10^{27}$ M^{-4}, and its calculated spectrum shows a Soret band at 429 nm, the UV−vis signature for a DABCO sandwich complex. The assembly of the cage **7** can be described in terms of a unique intermolecular association constant (K_m) and two EM values (eq 1).[7,8,27]

$$K_{32} = K_m{}^6 \mathrm{EM}_1 \mathrm{EM}_2 \quad (1)$$

The equilibrium constant for the intermolecular interaction between a zinc porphyrin and one nitrogen atom of DABCO was calculated from the interaction of **2** with DABCO as $K_m = K_{11}/2 = 6.5 \pm 0.5 \times 10^4$ M^{-1}, and the binding properties of the three porphyrins in the trimer **1** are assumed to be identical to this interaction. The experimental values of K_{32} and eq 1 allow us to calculate the product of $\mathrm{EM}_1\mathrm{EM}_2 = K_{32}/K_m{}^6 = 0.11 \pm 0.03$ M^2. Thus, the geometric average of the EM values for the two intramolecular cyclization processes is 0.3 M, which is identical to the EM value obtained for the single intramolecular cyclization observed in the assembly of the dimer sandwich complex, (DABCO)$_2$·**3**$_2$.[28] This strongly suggests that there is no significant difference between the two intramolecular steps involved in the assembly of the cage; that is, the final cage closure interaction is no more favorable than the first intramolecular cyclization process. So why are there no signs of partially formed or frayed intermediates during the UV−vis titrations? To understand the reasons, we need to estimate the stability constants for possible intermediates using eqs 2 and 3[29] and assuming that $\mathrm{EM}_1 = 0.3$ M.[30]

$$K_{22} = 9K_m{}^4 \mathrm{EM}_1 = 5 \times 10^{19}\ \mathrm{M}^{-3} \quad (2)$$

$$K_{42} = 36K_m{}^6 EM_1 = 9 \times 10^{29}\ \mathrm{M}^{-5} \quad (3)$$

Using these stability constants and the program SPECFIT, we simulated the speciation profile during the UV−vis titration of **1** (porphyrin concentration $\sim 10^{-6}$ M) with DABCO assuming that **1** is involved in five stoichiometric states: free **1**, (DABCO)$_2$·**1**$_2$, (DABCO)$_3$·**1**$_2$, (DABCO)$_4$·**1**$_2$, and (DABCO)$_3$·**1** (Figure 6a). The populations of the 2:2 and 2:4 species are negligible, explaining the good fit obtained for the titration data to theoretical model shown in Scheme 2 (all-or-nothing self-assembly process). The relative stability of all intramolecular complexes depends on the concentration at which the titration experiment is carried out. Figure 6b shows the simulated speciation profiles using the same binding model but in the millimolar concentration (1×10^{-3} M trisporphyrin **1**) regime of ^{1}H NMR experiments. The populations of the two intermediate species are significantly higher at millimolar concentrations of **1** (Figures 6b). At this concentration, both formation and destruction of cage **7** are predicted to occur simultaneously with the presence of the intermediate species which, in this case, are formed at a detectable concentration.

To gather experimental evidence for the presence of these intermediate species, we studied the complexation of DABCO to trisporphyrin **1** at millimolar concentrations using ^{1}H NMR spectroscopy. At room temperature in the presence of up to 1.5 equiv of DABCO, the chemical exchange process between free **1** and the complexed species is slow on the NMR time scale (Figure 7). Only one new set of signals is observed in the aromatic region of the ^{1}H NMR spectrum, and the methylene protons of DABCO appear as a unique singlet at $\delta = -5$ ppm, diagnostic of a sandwich complex. There is no clear evidence for the presence of a distinct species that can be assigned as the intermediate 2:2 complex predicted by the simulation. At 1.5 equiv of DABCO, only the new set of signals assigned to the cage complex **7** is observed. When more DABCO is added, the signal at $\delta = -5$ ppm broadens, and the porphyrin signals gradually shift, indicating fast exchange between the self-assembled cage **7** and opened complexes. Again, there are no obvious signs of an intermediate.

In an attempt to identify possible intermediate species, we decided to work at low temperature to slow the exchange processes between different complexes. When the second destruction phase of the titration was studied at 250 K, no new species were observed. All signals were broad and poorly resolved. The first phase of the titration (0−1.5 equiv of DABCO) was studied at 230 K. The aromatic region is very complex, and the signal due to the methylene protons of the sandwiched DABCO at $\delta = -4.91$ ppm is much broader than that at room temperature. In the presence of 0.9 equiv of DABCO, two different signals in slow exchange are observed: one is broad at $\delta = -4.91$ ppm, and there is another sharper

(26) $K_m = 6.5 \pm 0.5 \times 10^4$ M^{-1} is the calculated microscopic constant for the interaction of DABCO with **2** from which statistical effects have been removed. The statistical correction of 8 reflects the degeneracy of the complex. Each monocoordinated DABCO ligand has two possible arrangements which give a total of eight possible arrangements for the complex ($2 \times 2 \times 2$). The cooperativity factors for trisporphyrin **1** on binding quinuclidine to form a 3:1 complex were calculated to be close to 1 and are assumed to be similar to that for binding DABCO. A clear indication of the quality of the fit comes from the fact that if K_{31} is not fixed a similar value is obtained (1.95×10^{15} M^{-3}).

(27) Ercolani, G. *J. Am. Chem. Soc.* **2003**, *125*, 16097−16103.

(28) The reported effective molarity values (EM) are not statistically corrected due to the difficulty of evaluating unequivocal symmetry numbers for the flexible molecules at hand. Statistically corrected (or microscopic) EM_m values are necessary for comparison among different systems, but they are not relevant for the conclusions of this work. Any statistical correction will lower the reported values of EM, but they will still be identical within experimental error. For examples of statistically corrected effective molarities, see refs 6 and 27.

(29) The statistical correction included in eqs 2 and 3 comes from the degeneracy of the complexes. There are nine degenerate 2:2 complexes because each of the three porphyrins in each trimer can occupy the "free" position in the complex (3×3). In the 4:2 complex, there is additional degeneracy (2×2) due to the monocoordinated DABCO ligands that have four possible arrangements.

(30) The calculated values for the stability constants K_{22} and K_{42} using the methodology described in the Supporting Information are in accordance with the estimated statistical constants.

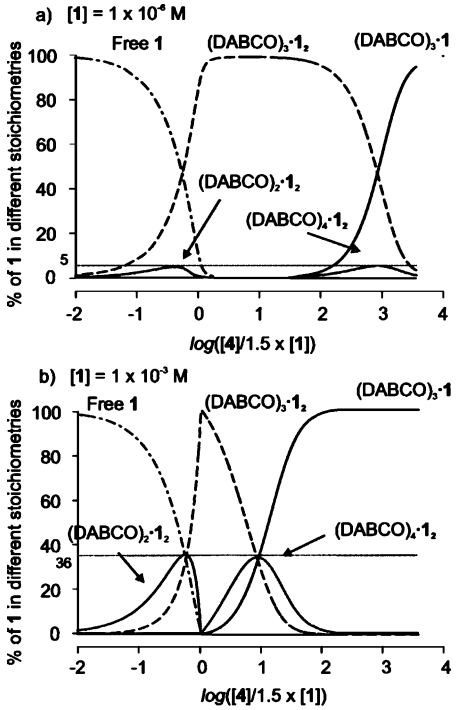

Figure 6. Simulated speciation profiles for titrations of **1** with DABCO (**4**). (a) [**1**] = 1×10^{-6} M and (b) [**1**] = 1×10^{-3} M.

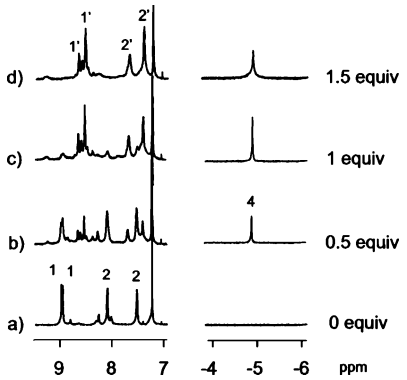

Figure 7. Selected regions of the ^{1}H NMR spectra recorded during a titration of **1** ([**1**] = 5×10^{-4} M) with DABCO (number of equivalents added are indicated). Signals labeled 1 and 2 represent the β-pyrrole and the aromatic protons of the *meso*-phenyl substituent of free **1**, respectively; primed numbers indicate the same signals in the (DABCO)$_3$·**1**$_2$ cage complex (**7**). The signal labeled 4 represents the DABCO methylene protons in a sandwich complex.

signal at $\delta = -4.94$ ppm (Figure 8a). When more DABCO is added, the signal at $\delta = -4.94$ ppm grows at the expense of the signal at $\delta = -4.91$ ppm. When 1.5 equiv of DABCO is present, only the signal at $\delta = -4.94$ ppm is observed, which we assign to the methylene protons of DABCO in cage **7**. The broader signal at $\delta = -4.91$ ppm is therefore assigned to the less stable 2:2 intermediate predicted by the simulation above. Figure 8b shows the deconvolution of the two signals that can be used to quantify the populations of the two complexes. The simulated speciation profiles simulated using the stability constants discussed above are in considerable agreement with the experimental populations from the deconvolution (Figure 8c). These observations unequivocally prove the existence of two different sandwich complexes in solution.

Thus, the self-assembly process at micromolar concentrations displays an apparent all-or-nothing two-state assembly because of the relatively low concentrations of the intermediate species that can be detected at millimolar concentrations. The self-assembly process can be considered to be *cooperative* because at low concentrations assembly of the cage occurs exclusively with no significant population of intermediate species stabilized by fewer interactions. However, at higher concentrations, a stepwise assembly process with significant population of an intermediates species dominates.

Molecular Recognition within the Self-Assembled Coordination Cage 7. At millimolar concentrations, the addition of 1.5 equiv of DABCO to trisporphyrin **1** induces the self-assembly of cage **7** as the exclusive species in solution. We can therefore investigate its ability to function as a molecular receptor using ^{1}H NMR spectroscopy. Molecular modeling[33] indicates that the cage can adopt conformations featuring a binding pocket of considerable dimensions in which up to six amide groups converge. The flexibility of the cage allows breathing of the cavity height between dimensions of 0 to 7 Å (Figure 9).

Such a large, flexible and functionalized cavity should bind molecules having complementary size and shape through an induced fit mechanism. It is known that benzene-1,3,5-tricarboxamide packs in the solid state to form π-stacked rods encased in triple helical hydrogen bonded amide strands.[34] Since the molecular spacer used for the construction of trisporphyrin **1** is a benzene-1,3,5-tricarboxamide, a benzene ring with secondary amides at the 1,3,5-positions should be a suitable guest. Figure 10 shows the minimized structure[31] of the complex formed between **7** and *N*,*N*′,*N*″-tris(phenyl)benzene-1,3,5-tricarboxamide. Up to six hydrogen bonds can be formed between the two benzene-1,3,5-tricarboxamide units acting as the floor and ceiling of the multimolecular cage **7** and the benzene-1,3,5-tricarboxamide unit bound into the cavity forming a triple helical hydrogen bonding motif.

To examine experimentally the capability of cage **7** to act as a molecular receptor, we prepared a deuteriochloroform solution containing trisporphyrin [**1**] = 5×10^{-4} M and added 1.5 equiv of DABCO. The full assembly of cage **7** was confirmed using ^{1}H NMR spectroscopy (Figure 11).

Next, incremental amounts of tricarboxamide **9**[35] or **10** dissolved in deuteriochloroform were titrated into the cage solution. Unfortunately, most proton signals of **7** broaden on addition of the guest, probably due to exchange between free and bound species. The signal assigned to the NH protons of the cage disappears due to broadening after 1.7 equiv of the tricarboxamide has been added. This dynamic behavior makes it difficult to quantify the molecular recognition capabilities of cage **7** toward the tricarboxamides **9** or **10** using ^{1}H NMR spectroscopy.

Nevertheless, the chemical shift changes experienced by the cage and tricarboxamide protons during the complexation

(31) *PeakFit* v4.12 for Windows.
(32) The simulated profiles are derived from the stability constants determined at 298 K and are used to overlay with the experimental data obtained at 230 K.
(33) *CAChe WorkSystem*, cersion 6.1.12.33; Fujitsu Limited.
(34) Lightfoot, M. P.; Mair, F. S.; Pritchard, R. G.; Warren, J. E. *Chem. Commun.* **1999**, 1945−1946.
(35) Tricarboxamides **9** and **10** tend to aggregate in chloroform solution. We calculated a dimerization constant, $K_d = 100$ M^{-1}, using ^{1}H NMR spectroscopy. Since the titration of the cage with tricarboxamide **9** or **10** was performed at almost constant millimolar concentration of tricarboxamide, we consider the possible effect of the dimerization on the binding constant to be almost negligible.

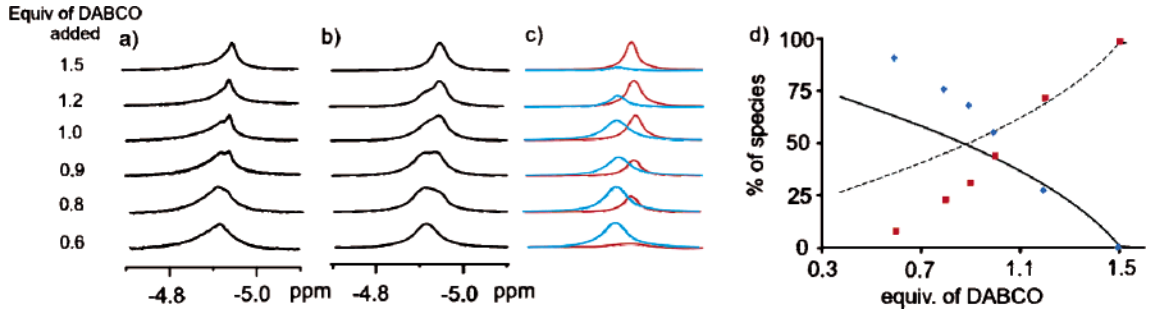

Figure 8. (a) Expansion of the −5 ppm region of the ^{1}H NMR spectra recorded during a titration of **1** with DABCO ([**1**] = 5 × 10^{-4} M) at 230 K in $CDCl_3$. (b) Simulated spectra obtained by simple deconvolution assuming two signals at $\delta = -4.91$ and −4.94 ppm.[31] (c) The deconvoluted signals that give rise to the simulated spectra in (b) that we assign to the 2:2 (blue) and 2:3 (red) complexes. (d) Simulated speciation profiles for the 2:2 (solid line) and the 2:3 (dashed line) species during a titration of **1** ([**1**] = 5 × 10^{-4} M) with DABCO (0.4−1.5 equiv) and experimental populations based on integration of the deconvoluted signals assigned to the 2:2 (diamonds) and 2:3 (squares) species.[32]

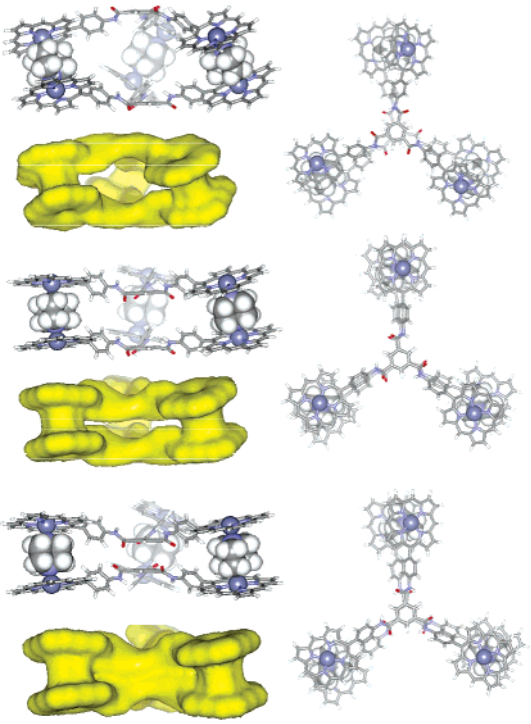

Figure 9. Molecular mechanics optimized structures (CAChe, MM3 force field)[31] of cage **7** in three representative conformations. The porphyrin *meso*-phenyl groups are truncated to a hydrogen atom for clarity. The drawings are a side view, a soft solvent surface (probe radius 1.4 Å) of the side view, and a top view for each of three conformations. In the conformation at the top, the six oxygen atoms of the benzene-1,3,5-tricarboxamide spacer are pointing outside of the cavity (distance between aromatic spacers = 11 Å). In the middle conformation, three oxygen atoms point inside and three outside of the cavity (distance between aromatic spacers = 6.8 Å), and in the bottom example, all six oxygen atoms point inside, collapsing the cavity.

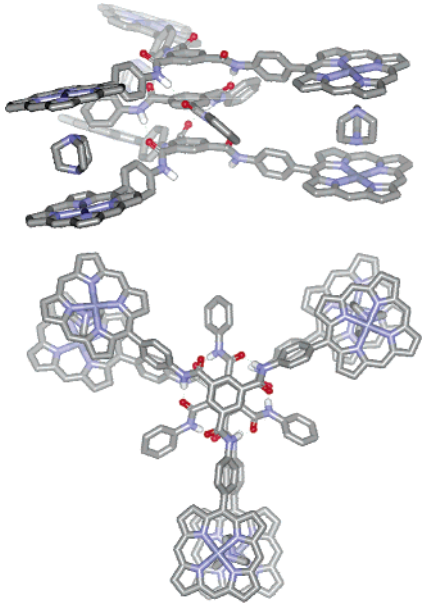

Figure 10. Side and top view of the minimized molecular structure (CAChe, MM3) of *N*,*N*′,*N*″-tris(phenyl)benzene-1,3,5-tricarboxamide@**7**. *meso*-Phenyl groups and nonpolar hydrogens have been omitted for clarity.

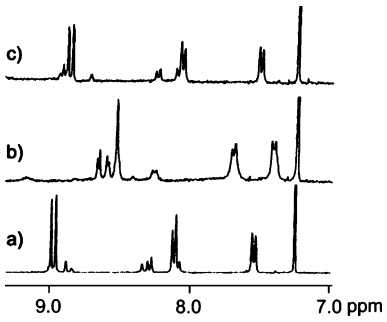

Figure 11. Expansions of the aromatic region of the ^{1}H NMR spectra of (a) trisporphyrin [**1**] = 5 × 10^{-4} M, (b) cage **7** ([**1**] = 5 × 10^{-4} M; [**DABCO**] = 7.5 × 10^{-4} M), and (c) open complex **8** ([**1**] = 5 × 10^{-4} M; [**DABCO**] = saturated solution). The assembly of cage **7** in (b) is clearly confirmed by ^{1}H NMR spectroscopy.

experiment reveal some information about the structure of the complex. The downfield shift of 0.1 ppm observed for both the NH protons of cage **7** and tricarboxamide **10** indicates the formation of a hydrogen bonded complex. Additionally, the aromatic proton of tricarboxamide **10** is shifted upfield, indicative of aromatic stacking. Although most of the signals due to the free receptor cage **7** and the complexed cage **10**@**7** are in intermediate exchange on the NMR time scale, the signals due to the methylene protons of the DABCO component are in slow exchange. As shown in Figure 13, the addition of **10** to a solution of **7** leads to the appearance of a new broad signal at −5 ppm. This signal increases at the expense of the original DABCO signal due to free cage **7** ($\delta = -4.55$ ppm), so the new signal is assigned to the DABCO protons in the **10**@**7** complex. Lowering the temperature also influences the ratio of these two signals. At lower temperature, the formation of the complex is favored due to the reduction of the entropic term, and consequently, the signal assigned to the methylene protons of DABCO in the **10**@**7** complex increases. These observations together with the high value determined for the association

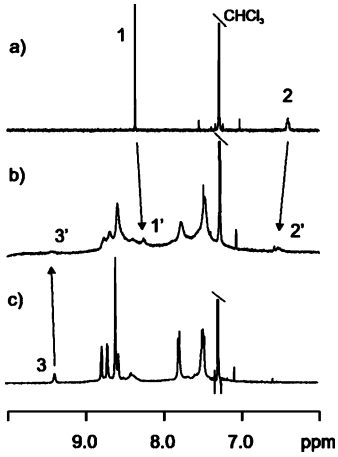

Figure 12. Part of the ^{1}H NMR spectra (500 MHz, $CDCl_3$) at 303 K of (a) guest tricarboxamide [**10**] = 5.3×10^{-4} M, (b) a solution containing cage [**7**] = 4.1×10^{-4} M and tricarboxamide [**10**] = 5.3×10^{-4} M, (c) receptor cage [**7**] = 4.1×10^{-4}. The signals labeled as 1 and 2 are assigned to the aromatic protons and NHs of tricarboxamide **10**, respectively. The signal labeled as 3 is assigned to the NHs of cage **7**. The primed signals indicate the corresponding protons in the mixture.

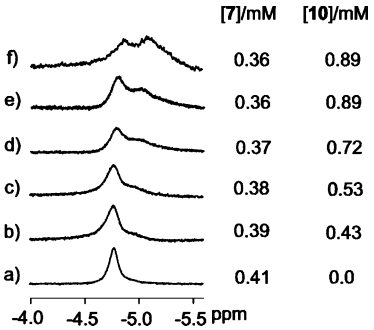

Figure 13. Expansion of the upfield region of the ^{1}H NMR (500 MHz, $CDCl_3$) spectra of (a) receptor cage **7**; (b−e) solutions containing cage **7** and tricarboxamide **10** at 303 K, (f) same as (e) but recorded at 230 K. The two broad signals shown here are assigned to DABCO methylene protons in the free cage **7** ($\delta = -4.55$ ppm) and in the complexed cage in **10**@**7** ($\delta = -5$ ppm).

constant for the **10**@**7** complex (vida infra) point toward an intracavity geometry, as shown in Figure 10.[36]

Isothermal titration calorimetry (ITC) is an alternative technique, which recently has attracted considerable attention, for the study of binding processes in solution.[37] ITC measurements allow the direct determination of the association constant, K_a, and the binding enthalpy, $\Delta H°$, providing a complete thermodynamic picture of the interaction under investigation. Calorimetric titrations were performed by adding a chloroform solution of cage **7** to a chloroform solution of the tricarboxamide (**9** or **10**). The results are very similar for both tricarboxamides (Table 1), and only the ITC data for **10** will be discussed in detail.

(36) An extra-cavity complex will be stabilized by just three hydrogen bonds and a single aromatic interaction. It is expected to show fast exchange on the NMR time scale and a stability constant in the order of 10^2 M^{-1}. The outer cavity geometry complex will produce a small modification on the magnetic environment of the DABCO protons.

(37) Examples of ITC applicability to supramolecular chemistry and host−guest recognition: (a) ten Cate, M. G. J.; Huskens, J.; Crego-Calama, M.; Reinhoudt, D. N. *Chem.—Eur. J.* **2004**, *10*, 3632−3639. (b) Kerckhoffs, J.; ten Cate, M. G. J.; Mateos-Timoneda, M. A.; van Leeuwen, F. W. B.; Snellink-Ruel, B.; Spek, A. L.; Kooijman, H.; Crego-Calama, M.; Reinhoudt, D. N. *J. Am. Chem. Soc.* **2005**, *127*, 12697−12708. (c) Jadhav, V. D.; Schmidtchen, F. P. *Org. Lett.* **2005**, *7*, 3311−3314. (d) Tobey, S. L.; Anslyn, E. V. *J. Am. Chem. Soc.* **2003**, *125*, 10963−10970. (e) Ballester, P.; Costa, A.; Deyà, P. M.; Vega, M.; Morey, J.; Deslongchamps, G. *Tetrahedron Lett.* **1999**, *40*, 171−174.

Table 1. ITC Data for the Complexation of Benzene-1,3,5-tricarboxamides **9** and **10** by the Coordination Cage **7** at 295 K

guest	K_a (10^3 M^{-1})	$\Delta G°$ (kcal·mol^{-1})	$\Delta H°$ (kcal·mol^{-1})	$T\Delta S°$ (kcal·mol^{-1})
9	9 ± 0.1	−5.3	-19.0 ± 0.4	−13.7
10	14 ± 1.5	−5.6	-13.4 ± 0.2	−7.8

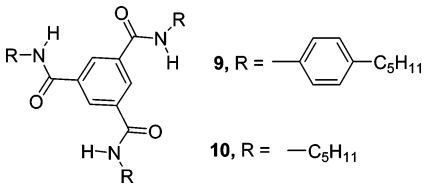

Figure 14. Molecular structure of benzene-1,3,5-tricarboxamides **9** and **10**.

Figure 15a depicts the (exothermic) heat evolved per injection plotted against the molar ratio for the calorimetric titration of **7** ([**7**] = 5 mM) with **10** ([**10**] = 0.5 mM). The binding isotherm is sigmoidal and shows an inflection point at a molar ratio of approximately 0.7, suggesting a single binding event and a simple 1:1 stoichiometry for the complex being formed (**10**@**7**). The control experiment injecting cage **7** ([**7**] = 5 mM) into chloroform (Figure 15a top trace) showed a very small and almost constant endothermicity due to dilution.

The heat of the dilution experiment was subtracted from the heat of the binding experiment, and the result was fit to a 1:1 binding model (Figure 15b) to give a binding constant of $K_a = 1.4 \times 10^4$ M^{-1}. Formation of **10**@**7** is strongly enthalpy ($\Delta H° = -13.4 \pm 0.2$ kcal·mol^{-1}) driven. The observed negative enthalpy change likely occurs from the formation of hydrogen bonds and favorable aromatic interactions in the complex. Assuming an enthalpy gain of 2 kcal·mol^{-1} per hydrogen bond formed in chloroform, the observed enthalpy for the complex is in agreement with the formation of six good N−H···O=C hydrogen bonds.[38] The adverse negative entropy ($T\Delta S° = -7.8$ kcal·mol^{-1}) probably arises from a loss of conformational entropy on complex formation and changes in conformational mobility of both host and guest.

Another reference ITC measurement was performed to ascertain that the exothermic profile observed for the titration of tricarboxamide **10** with cage **7** (Figure 15b) was really due to the existence of a binding process between these two species. Thus, the injection of trisporphyrin **1** ([**1**] = 6.2 mM) to a chloroform solution of tricarboxamide **10** ([**10**] = 0.455 mM) gave a heat profile (Figure 16a) similar to that obtained for the simple dilution experiment of trisporphyrin **1** (Figure 16b). On one hand, this result indicates that tricarboxamide **10** does not interact with trisporphyrin **1**, one of the components of cage **7**, and proves that the ITC binding isotherm of the titration of cage **7** with tricarboxamide **10** is due to the complex formation **10**@**7**. On the other hand, the different profiles for the dilution curves obtained with cage **7** (Figure 15a top trace) and trisporphyrin **1** (Figure 16b) demonstrate that under these conditions the dimerization processes of these two species are very different. The dimerization constant and the dimerization enthalpy of trisporphyrin **1** ($K_d = 1.1 \pm 0.1 \times 10^{-3}$ M and $\Delta H°_{dis} = 14.1$

(38) Hunter, C. A. *Angew. Chem., Int. Ed.* **2004**, *43*, 5310−5324.

(39) A constant value of 28 μcal has been added to each data point plotted in the graphs to account for the injection heat.

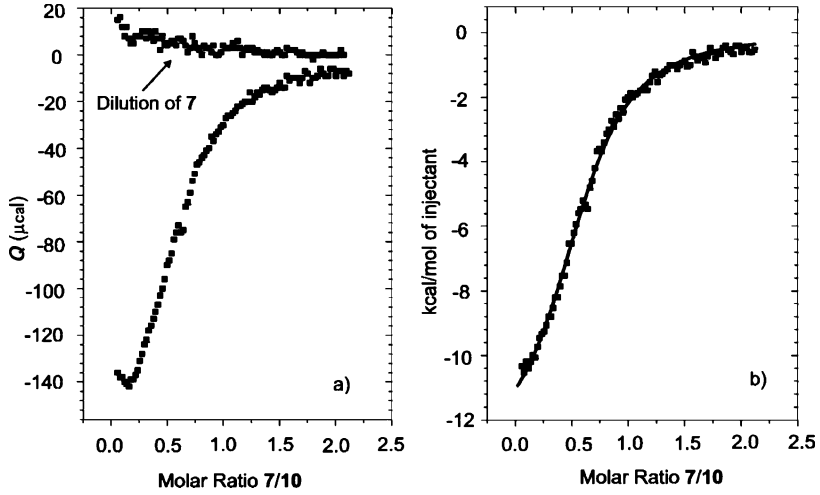

Figure 15. ITC measurements (a) for the formation of the complex **10**@**7** and for the dilution of **7** (top trace); (b) final binding isotherm for the formation of the complex **10**@**7** fitted to a 1:1 binding algorithm.

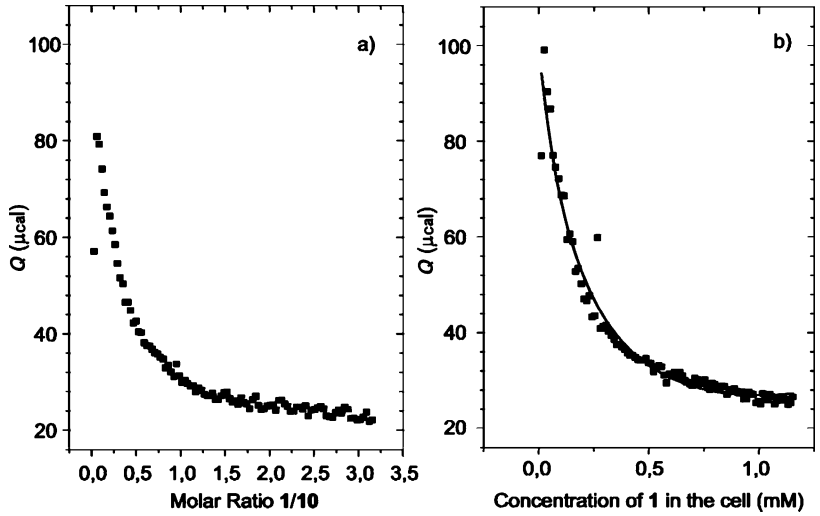

Figure 16. ITC measurements (a) for the titration of trisporphyrin **1** with tricarboxamide **10** and (b) for the dilution of **1** fitted to a dimer dissociation model.[39]

± 0.1 kcal·mol^{-1}, respectively) were calculated using the dimer dissociation model implemented in Microcal ITC Data Analysis software.

Conclusions

In summary, we have shown that, at micromolar concentrations, the coordination of trisporphyrin **1** with 1,4-diazabicyclo-[2.2.2]octane (DABCO) forms a stable $(DABCO)_3$:$\mathbf{1}_2$ double-decker molecular cage **7**, and when excess DABCO is added, cage **7** collapses to yield a simple open complex $(DABCO)_3$:**1**. We have been able to quantitatively characterize the binding process of **1** with DABCO in terms of a single stability constant (K_m) that describes the strength of the individual coordination interactions and two effective molarities (EM) that describe the additional stability imparted by intramolecular cyclization. The two EM values calculated for the consecutive cyclic intramolecular interactions involved in the assembly of **7**, EM_1 and EM_2, are very similar. We were not able to detect the formation of intermediate species at micromolar concentrations. To clarify this point, we have estimated the stability constants of possible intermediate species $(DABCO)_2$:$\mathbf{1}_2$ and $(DABCO)_4$:$\mathbf{1}_2$ using the thermodynamic parameters (K_m and EM_1) and simulated speciation profiles of **1** with DABCO at different concentrations. If we compare the simulation in the micromolar regime with that in the millimolar regime, there is a clear dependency of the relative percentage of intermediate species with concentration because the stability advantage imparted by any intramolecular interaction is concentration dependent. The stabilities of the intermediate species $(DABCO)_2$:$\mathbf{1}_2$ and $(DABCO)_4$:$\mathbf{1}_2$ increase significantly with concentration. Therefore, "all-or-nothing" behavior is only observed at micromolar concentrations, where intermediates attain very low concentrations. At millimolar concentrations, the increase in the concentration of the intermediates moves the systems into a stepwise behavior. Experimentally, we have been able to detect the $(DABCO)_2$:$\mathbf{1}_2$ intermediate at millimolar concentrations using ^{1}H NMR spectroscopy. Thus, the observed all-or-nothing behavior is not due to more favorable sequential intramolecular cyclizations, but to the combination of high EM values with low concentrations used to carry out the study. We imply that this could be a general scenario found in many artificial self-assembling systems displaying this type of behavior.

The cage complex **7** features a large well-defined cavity in which up to six amide groups can converge. We have shown

that cage **7** is a supramolecular host capable of forming intracavity complexes with benzene-1,3,5-tricarboxamide derivatives (**9** and **10**). The driving force for complexation is the establishment of six N−H···O═C hydrogen bonds and additional favorable aromatic interactions. ITC measurements allowed the quantification of the free energies of complexation, $\Delta G°$, which are of the order of -5 kcal·mol^{-1}, as well as the 1:1 stoichiometry assigned to the complex. Controlling the number of molecules that can be accommodated in the interior of the cavity by changing the length of the diamine ligand is currently under investigation.

Acknowledgment. We thank Dirección General de Investigación, Ministerio de Ciencia y Tecnología (BQU2002-04651 and CTQ2005-08989-C02/BQU) for grant support. P.B. and A.I.O. also thank ICIQ Foundation and DURSI (Grant 2005SGR00108) for financial support.

Supporting Information Available: Brief description of the techniques used to carry out the UV−vis, ^{1}H NMR, and ITC titrations mentioned in the text, and the corresponding data fit. Experimental procedures used for the synthesis of trisporphyrin **1**. Description of the methodology referred to in ref 28 for the calculation of the stability constants of the intermediate species $(DABCO)_3$·$\mathbf{1}_2$ and $(DABCO)_4$·$\mathbf{1}_2$. This material is available free of charge via the Internet at http://pubs.acs.org.

JA060608T